JACS
JOURNAL OF THE AMERICAN CHEMICAL SOCIETY
Article
pubs.acs.org/JACS

Antigenic Peptide Recognition on the Human ABC Transporter TAP Resolved by DNP-Enhanced Solid-State NMR Spectroscopy

Elisa Lehnert,[†,∥] Jiafei Mao,[‡,∥] Ahmad Reza Mehdipour,[§] Gerhard Hummer,[§] Rupert Abele,[†] Clemens Glaubitz,[*,‡] and Robert Tampé[*,†]

[†]Institute of Biochemistry, Biocenter, [‡]Institute for Biophysical Chemistry and Centre for Biomolecular Magnetic Resonance, Goethe University Frankfurt, Max-von-Laue-Str. 9, 60438 Frankfurt am Main, Germany

[§]Department of Theoretical Biophysics, Max Planck Institute of Biophysics, Max-von-Laue-Str. 3, 60438 Frankfurt am Main, Germany

Supporting Information

ABSTRACT: The human transporter associated with antigen processing (TAP) is a 150 kDa heterodimeric ABC transport complex that selects peptides for export into the endoplasmic reticulum and subsequent loading onto major histocompatibility complex class I molecules to trigger adaptive immune responses against virally or malignantly transformed cells. To date, no atomic-resolution information on peptide−TAP interactions has been obtained, hampering a mechanistic understanding of the early steps of substrate translocation catalyzed by TAP. Here, we developed a mild method to concentrate an unstable membrane protein complex and combined this effort with dynamic nuclear polarization enhanced magic angle spinning solid-state NMR to study this challenging membrane protein−substrate complex. We were able to determine the atomic-resolution backbone conformation of an antigenic peptide bound to human TAP. Our NMR data also provide unparalleled insights into the nature of the interactions between the side chains of the antigen peptide and TAP. By combining NMR data and molecular modeling, the location of the peptide binding cavity has been identified, revealing a complex scenario of peptide−TAP recognition. Our findings reveal a structural and chemical basis of substrate selection rules, which define the crucial function of this ABC transporter in human immunity and health. This work is the first NMR study of a eukaryotic transporter protein and presents the power of solid-state NMR in this growing field.

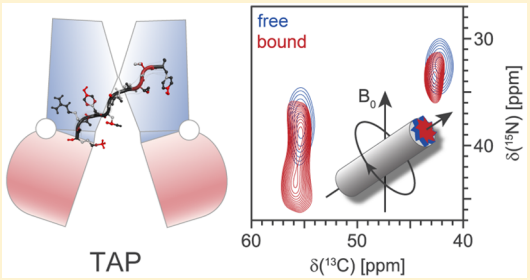

INTRODUCTION

ATP-binding cassette (ABC) transporters belong to the family of primary active transporters that utilize the energy from ATP hydrolysis to shuttle molecules across a membrane against a concentration gradient. ABC transporters are found in all kingdoms of life, where they fulfill diverse functions as exporters and importers, such as nutrition uptake, lipid trafficking, ion homeostasis, multidrug resistance, signal transduction, and antigen processing. In bacteria, ∼2% of genes code for ABC transporters, whereas 48 human ABC proteins exist.[1] The transporter associated with antigen processing (TAP) is a key player in the adaptive immune system, which vested vertebrates with sophisticated strategies to detect and eliminate virus infected or malignantly transformed cells. Within this cellular process, TAP predominantly selects proteasomal degradation products for translocation and loading onto major histocompatibility complex class I (MHC I) molecules in the endoplasmic reticulum (ER) lumen. Subsequently, the peptide−MHC I complexes travel to the cell surface to present their antigenic cargo to cytotoxic T cells.[2,3] The TAP complex is composed of TAP1 (ABCB2) and TAP2 (ABCB3), each consisting of a transmembrane domain (TMD) and a nucleotide binding domain (NBD) facing the cytosol. Each half-transporter contains an extra N-terminal four-transmembrane helix bundle, called TMD0,[4] which is indispensable for the assembly of the macromolecular peptide-loading complex.[5] The coreTAP complex lacking these TMD0s is essential and sufficient for peptide binding and translocation.[5,6]

The peptide binding site of the TAP complex has been narrowed down to the cytosolic loops between TM4 and TM5 in addition to a linker region between the TMD and NBD of each subunit.[7,8] The antigen translocation machinery binds peptides of 8−16 amino acids with nanomolar affinity.[9] The free N and C termini as well as three N-terminal residues and the C-terminal residue are critical for peptide binding.[10−13] The region between these "anchor" residues can be promiscuous in sequence and length. EPR spectroscopy revealed a distance of ∼2.5 nm between the N and C terminus of the peptide independent of the peptide's length.[13]

Despite these efforts, the true nature of substrate−TAP interactions and epitope selection is not yet understood. In particular, the conformation of the peptide cargo in the TAP substrate binding pocket has not been resolved. In general, structural insights into bound substrates and their binding sites are crucial to understand the substrate selection, sequence

Received: July 24, 2016
Published: September 23, 2016

DOI: 10.1021/jacs.6b07426
J. Am. Chem. Soc. 2016, 138, 13967−13974

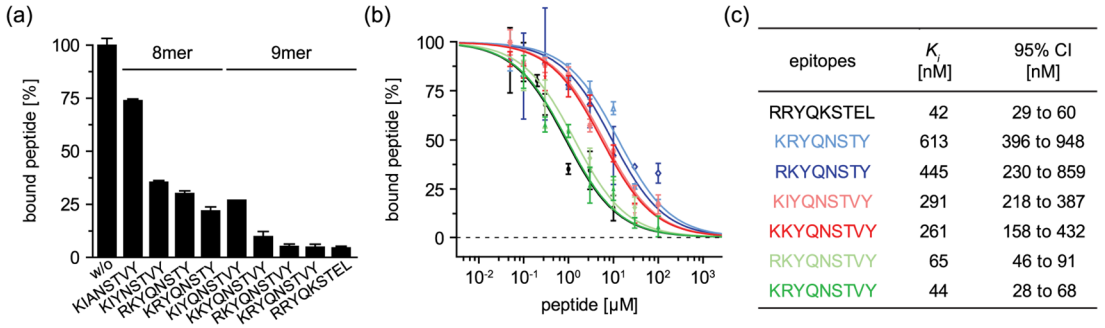

epitopes	K_i [nM]	95% CI [nM]
RRYQKSTEL	42	29 to 60
KRYQNSTY	613	396 to 948
RKYQNSTY	445	230 to 859
KIYQNSTVY	291	218 to 387
KKYQNSTVY	261	158 to 432
RKYQNSTVY	65	46 to 91
KRYQNSTVY	44	28 to 68

Figure 1. Competition of peptide binding to TAP by designed 8- and 9-mer peptides. (a, b) In a fluorescence-based filter assay, the reporter peptide (1 μM, RRYC^{F}KSTEL) was competed by a 250-fold excess (a) and increasing concentrations of optimized peptides using purified TAP (b). Error bars: SD. (c) From the competition curves, the IC_{50} values were deduced and converted to an inhibition constant (K_i) using the Cheng–Prusoff equation and a K_D of 50 nM for the reporter peptide. Errors are indicated as the confidence interval (CI).

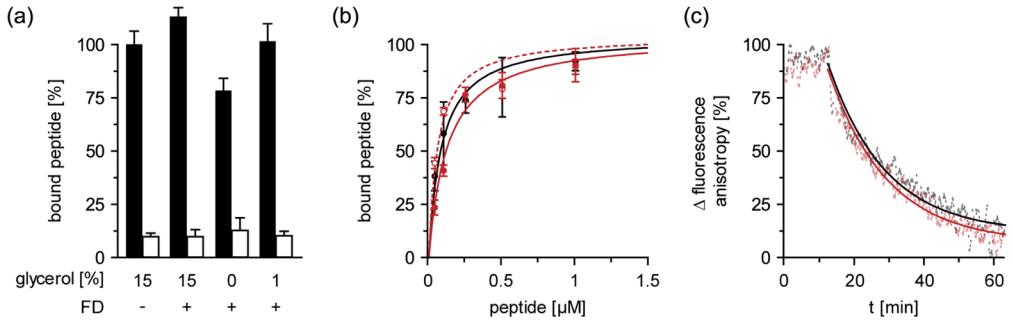

Figure 2. The condensed glycerol matrix yields a highly concentrated active TAP complex. (a) Activity of TAP before and after freeze-drying (FD) at given concentrations of glycerol. TAP (175 nM) was adjusted to different glycerol concentrations, snap-frozen, and freeze-dried. Samples were rehydrated to the original volume, and TAP was incubated with fluorescently labeled peptide (1 μM, RRYC^{F}KSTEL; black bar) in the presence or absence of competitor peptide (250 μM, RRYQKSTEL; white bar). (b) Freeze-drying disturbs neither the TAP binding capacity (B_{max}) nor the peptide affinity (K_D). Binding affinities were determined before (black line) or after freeze-drying of TAP (175 nM, red line) with increasing concentrations of fluorescent peptide (RRYC^{F}KSTEL) in the presence or absence of competitor peptide (250 μM, RRYQKSTEL) in a buffer containing 1% glycerol. To demonstrate that the peptide remained in complex with TAP in the freeze-dried state, TAP was preincubated with the indicated concentration of fluorescent peptide, freeze-dried, and subsequently rehydrated in 5 volumes of water containing unlabeled competitor (250 μM, RRYQKSTEL; dashed red line) to prevent rebinding of dissociated reporter peptide. Data were fitted by the Langmuir (1:1) isotherm, resulting in equilibrium dissociation constants K_D of 87 ± 14 nM (untreated TAP) as well as 127 ± 21 and 61 ± 16 nM for freeze-dried TAP complexes in the presence or absence of peptide, respectively. Binding data normalized to untreated TAP reflect the mean of triplicates, and error bars indicate SD. (c) Freeze-drying has no influence on peptide binding kinetics. Fluorescent peptide (50 nM, RRYC^{ATTO565}KSTEL) was preincubated with TAP (1.35 μM) untreated (black line) or freeze-dried (red line). After reaching equilibrium, a 1500-fold excess of unlabeled competitor peptide RRYQKSTEL was added to follow the peptide dissociation kinetics. Fluorescence anisotropy ($\lambda_{ex/em}$ 563/592 nm) was recorded at 4 °C. Data fitted by a monoexponential function revealed a k_{off} of (0.96 ± 0.05) × 10^{-3} s^{-1} and (0.89 ± 0.04) × 10^{-3} s^{-1} for untreated and freeze-dried TAP, respectively.

polymorphism, and transport mechanism of ABC proteins involved in human disorders.

In fact, elucidating the crystal structure of the native substrate-bound states of ABC exporters has turned out to be quite a challenge and has not been successful so far. We therefore chose a different approach and directly analyzed the structure of a peptide substrate in human TAP by solid-state nuclear magnetic resonance (ssNMR) spectroscopy under magic angle spinning (MAS). To overcome the sensitivity limit of conventional ssNMR, we applied cross-effect dynamic nuclear polarization (DNP), by which dipole-coupled electron spin pairs hyperpolarize nearby protons under microwave irradiation (for a review, see ref 14) and boost NMR sensitivity. This technique has recently been used to explore a number of new biomolecular scenarios (for recent review, see ref 15), such as large membrane protein complexes within native membranes,[16] in-cell protein folding,[17] membrane protein interactions,[18] and metastable functional states.[19]

Encouraged by this exciting progress, we here adopt the DNP-ssNMR technique for high-resolution structural studies of eukaryotic membrane protein systems. The large signal enhancement offered by DNP makes it possible for us to probe a human transport complex. Our data defines the backbone conformation of the TAP-bound antigenic peptide at atomic resolution and decodes the substrate selection rules, which define the function of this human ABC transporter. Building upon the defined NMR structure model, a docking approach was applied to localize the peptide binding pocket and to identify key residues interacting with the peptide substrate, which now turns earlier sparse mutagenesis studies into a collective and mechanistic picture based on 3D structural models.

RESULTS

Reporter Peptides for NMR Analyses of Human TAP. The peptide epitope RRYQKSTEL derived from human histone H3.3 is presented on human leukocyte antigen HLA-

DOI: 10.1021/jacs.6b07426
J. Am. Chem. Soc. 2016, 138, 13967–13974

B27, which is strongly associated with inflammatory diseases.[20] This epitope binds with high affinity to the TAP complex (K_D = 50 nM).[21] The amino acid sequence, however, had to be optimized to reach broad signal dispersion and detectability of the side chain NMR signals under DNP conditions. In particular, the leucine side chain often enters an unfavorable motion regime at temperatures of about 100 K in DNP measurements, resulting in a drastic loss of signal intensity.[22] We thus substitute the C-terminal leucine by tyrosine, which is favored by TAP as its anchor position.[12]

Using Fmoc solid-phase synthesis, we systematically diversified peptide sequence and length with respect to NMR spectrum complexity, side chain detectability, and binding affinity (Figures 1 and S1). Despite identical anchor residues, 8-mer peptides display reduced affinities to TAP as compared to the corresponding 9-mer. In contrast to the high-affinity epitope, the 8-mers KRYQNSTY and RKYQNSTY showed K_i > 400 nM and are therefore not qualified for our NMR analyses. The binding affinity of the 9-mer peptides KIYQNSTVY and KKYQNSTVY improved slightly. Restoring the arginine at position 2 led to KRYQNSTVY with an affinity identical to the peptide RRYQKSTEL (Figure 1).

A Condensed Glycerol Matrix for DNP-Enhanced ssNMR of Biological Samples. DNP-enhanced ssNMR experiments were performed using the human coreTAP complex,[5] subsequently referred to as TAP. Despite the substantial signal enhancement provided by DNP, condensing a sufficient amount of protein into the 30 μL volume of a MAS rotor is challenging, especially for human multisubunit membrane protein complexes such as TAP. Functional reconstitution in liposomes at higher molar protein-to-lipid ratios (1:50−200), as routinely used for ssNMR studies on prokaryotic membrane proteins, could not be achieved for TAP. Detergent-solubilized TAP can be concentrated only up to 10 mg/mL (60 μM) by conventional procedures. A higher concentration results in aggregation and a loss of TAP activity. Unfortunately, this problem was circumvented neither by a sedimentation approach[23,24] nor by reconstitution into nanodiscs.[21] In addition, the protein has to be immersed in a glass-forming matrix, preventing the polarizing agents from aggregation. We therefore developed a new approach: Freshly isolated peptide−TAP complexes in 0.05% GDN detergent at different concentrations of glycerol were flash-frozen, and excess water was gradually removed by a freeze-drying procedure. To examine the TAP activity, samples were rehydrated and peptide binding was analyzed by filter binding and fluorescence anisotropy. In 15% glycerol, TAP activity was fully preserved (Figure 2a), but the sample was still too voluminous to fit into MAS rotors. Consequently, the glycerol content was reduced to 0 and 1%. In both cases, the sample volume could be reduced 100-fold; however, in the absence of glycerol, we observed significantly reduced TAP activity. Full binding capacity is retained in the case with a 1% initial glycerol concentration (Figure 2a). The applicability of our condensed glycerol matrix for DNP-enhanced solid-state NMR is in line with matrix-free sample preparations.[25]

As proof that TAP shows identical thermodynamics and kinetics of peptide binding after freeze-drying compared to untreated TAP, the complex was incubated with fluorescently labeled reporter peptide prior to or after freeze-drying. After rehydration of the freeze-dried peptide−TAP complex, the amount of specifically bound reporter was immediately determined to prevent peptide dissociation (Figure 2b). To exclude the possibility that TAP binds the peptide during rehydration, the freeze-dried peptide−TAP complex was rehydrated in a 250-fold molar excess of competitor. The identical amount of bound substrate in these experiments demonstrates that the peptide is bound to TAP in the freeze-dried state. The presence of unbound peptide can therefore be excluded. Similar K_D values for untreated or freeze-dried TAP complexes, the latter in the presence or absence of peptide of 87 ± 14, 127 ± 21, and 61 ± 16 nM, respectively, further confirmed TAP integrity in the freeze-dried state. In addition, peptide dissociation kinetics were followed by fluorescence anisotropy, revealing similar k_{off} rates of (0.96 ± 0.05) × 10^{-3} s^{-1} and (0.89 ± 0.04) × 10^{-3} s^{-1} for TAP prior to and after freeze-drying, respectively (Figure 2c). These substrate binding kinetics are in line with previous studies.[26] In conclusion, detergent-solubilized TAP can be concentrated in a glass-forming glycerol matrix to a concentration of 150 μM, where the substrate binding characteristics are fully preserved.

DNP-Enhanced ssNMR of the Peptide−TAP Complex. To obtain conformational and chemical information on the peptide in complex with TAP, we focused on ^{13}C and ^{15}N chemical shifts as the key NMR parameters. TAP was incubated with selectively isotope-labeled peptide KRYQNSTVY. Free peptides were removed by rapid gel filtration at 4 °C. After addition of AMUPol, a biradical polarizing agent,[27] and 1% glycerol, samples were immediately condensed as described above and transferred into the MAS rotor. DNP provided a 37-fold signal enhancement (Figure 3a). TAP integrity before and after NMR experiments was confirmed by identical peptide binding activities (Figure 3b). For the assignment of the ^{13}C and ^{15}N chemical shifts, two-dimensional $^{13}C-^{13}C$ DQ−SQ experiments using the POST-C7 scheme[28] and $^{15}N-^{13}C$

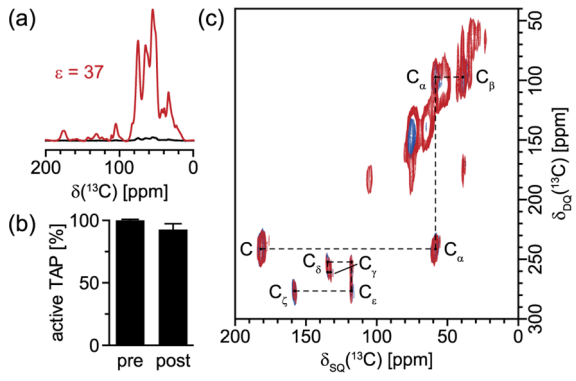

Figure 3. DNP-enhanced ssNMR studies of TAP-bound peptides. (a) ^{13}C MAS NMR spectra of TAP-bound ^{15}N,^{13}C Tyr selectively labeled KRYQNSTVY* with (red) or without (black) DNP show an approximately 37-fold enhancement (ε). (b) Peptide binding activity of untreated TAP (pre) and TAP rehydrated after the NMR measurement (post). TAP (175 nM), untreated or freeze-dried in complex with isotope-labeled KRYQNSTVY* used for NMR and rehydrated, was incubated with fluorescent peptide (270 μM, RRYC^{F}KSTEL) for 20 min at 4 °C, and the amount of active transporter was quantified by the fluorescence of the bound peptide. (c) 2D DQ−SQ spectra of KRYQNSTVY* free (blue) and bound to TAP (red). 4.5 nmol of TAP was incubated with 9 nmol of peptide. Peptide−TAP complexes were isolated by gel filtration, AMUPol was added, and TAP was concentrated by freeze-drying to approximately 30 μL (150 μM final). Dashed horizontal and vertical lines indicate sequential assignment walks. Additional signals between 65 and 110 ppm in the SQ dimension are derived from detergent.

DOI: 10.1021/jacs.6b07426
J. Am. Chem. Soc. 2016, 138, 13967−13974

TEDOR spectra[29,30] of differently labeled variants of the reporter peptide KRYQNSTVY, free and in complex with TAP, were recorded on a 400 MHz/263 GHz DNP spectrometer (Figures S2 and S3). Both types of experiments were selected because (i) they provide correlation spectra while suppressing natural abundance signals and (ii) the required magnetization transfer steps work with short mixing/excitation/reconversion times, minimizing the problem of a limited coherence lifetime in the presence of paramagnetic species. Six differently labeled KRYQNSTVY variants containing one or two uniformly ^{15}N,^{13}C-labeled amino acids were applied to reduce the spectral complexity. For example, the DQ–SQ spectrum of Tyr9 is shown in Figure 3c. Intraresidual assignment walks on the characteristic spectral patterns allowed the identification of ^{15}N and ^{13}C backbone and side chain chemical shifts of KRYQNSTVY in the free and transporter-bound state. Data are summarized in Tables S1 and S2.

Peptide Chemical Shift Changes upon Binding to TAP. The side chain signals of the free and transporter-bound peptide differ in 2D DQ–SQ and TEDOR ssNMR spectra. Notably, the three N-terminal residues and the C-terminal residue of the peptide are significantly affected upon TAP binding. Unexpectedly, the TEDOR signal of the N-terminal α-amino group of Lys1 splits within the ^{15}N dimension in the TAP-bound state, indicating the existence of two distinct conformations (Figure 4a). This surprising finding suggests a spatial freedom of the N terminus within the substrate binding pocket. Furthermore, peptide binding to TAP induces a small but significant ^{15}N downfield shift of the ε-amino group of Lys1. Both, the α- and ε-amino groups experienced a downfield shift (5.3 and 1.1 ppm), implying that they have a similar binding mode, possibly due to formation of hydrogen bonds between these primary amines and residues within the binding pocket of TAP. In contrast, the guanidinium group of Arg2 is hardly affected in the substrate binding site (Figure 4b). Chemical shifts of some phenyl ring carbons of Tyr3 and Tyr9 are influenced upon binding to TAP (Figures 4c, S2, and S3). In addition, the line width of the Tyr9 ζ position is significantly reduced upon binding (Tables S1 and S2). Residues between positions 4 and 8 displayed only slight or no observable changes in side chain chemical shifts upon TAP binding. In summary, the side chains of residues 1, 3, and 9 experience the most pronounced chemical shift changes upon TAP binding. At the backbone, some chemical shift changes were observed for Asn5, Thr7, and Val8 (Figure 4d), which might indicate that this part acts as a plastic linker for arranging the N- and C-terminal regions in different environments.

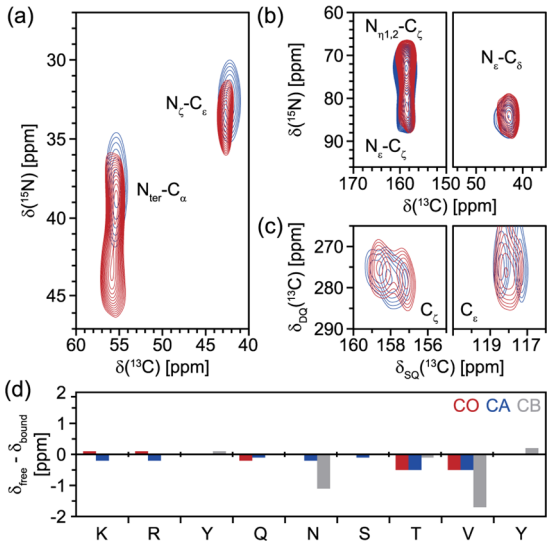

Figure 4. Chemical environment of the peptide backbone and side chain atoms differ in the free and TAP-bound state. 2D DQ–SQ or TEDOR correlation spectra of free (blue) and bound peptide (red) of the N-terminal and the ε-amino group of Lys1 (a), the guanidinium group of Arg2 (b), and the phenyl ring of Tyr9 (c). (d) Difference in chemical shifts of free and bound KRYQNSTVY of CO (red), CA (blue), and CB (gray).

Conformation of the TAP-Bound Peptide. Next, we determined the backbone conformation of free and transporter-bound peptides based on the NMR chemical shifts of the peptide backbone (CO, CA, N) and the β-position (CB) of each residue derived from 2D DQ–SQ or TEDOR spectra (Figure 4d). The range of possible backbone torsion angles predicted by TALOS-N[31] (Tables S3 and S4) served as restraints for calculating the structural model with CYANA.[32] The 10 lowest-energy peptide backbone structures of the TAP-bound and free state converged with root-mean-square deviations (RMSDs) of 0.63 and 0.59 Å, respectively (Figure 5). The comparison of both average structures resulted in an RMSD of 0.63 Å, indicating a similar overall backbone conformation for the free and bound peptide under our experimental conditions and within the structural resolution achievable by our data.

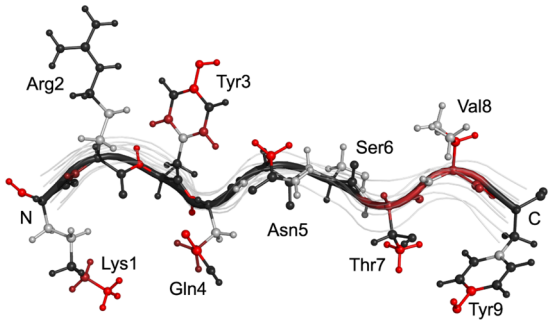

Figure 5. Backbone structure of a TAP-bound peptide. A representative backbone structure (black) of the 10 lowest-energy structures (light gray) of KRYQNSTVY was obtained from TALOS-N dihedral angle constraints following CYANA calculation.[31,32] Since the calculation does not permit side chain refinement, side chains are shown only for orientation purposes. The color gradient highlights atoms characterized by significant (red) and insignificant (gray) chemical shift changes upon peptide binding to TAP. Atoms without a detectable chemical shift are colored silver.

The DNP-enhanced NMR spectra of free and bound peptide feature complex line shapes with significant broadening (Tables S1 and S2). Our structure determination relied on analyzing the chemical shifts from the peak maxima, which were unambiguously determined for most nuclei and which represent the most populated conformation. The observed line broadening represents a high degree of peptide flexibility under room temperature conditions. The conformational space sampled by these motions would result in observing an averaged structure at room temperature, but it is trapped as a static ensemble under DNP conditions.

Our analysis shows that the 9-mer peptide binds to the TAP complex in an extended conformation (Figure 5). Secondary

DOI: 10.1021/jacs.6b07426
J. Am. Chem. Soc. 2016, 138, 13967–13974

structure motifs were not detected, which was confirmed by comparison with standard random coil backbone chemical shifts using CSI 2.0.[33] Structural changes in the peptide backbone upon binding to TAP were observed by altered chemical shifts at Asn5, Thr7, and Val8 (Figure 4d) and were especially pronounced for C_β of Asn5 and Val8. Moreover, the measured distance of 2.49 ± 0.03 nm between the N and C termini is in perfect agreement with the pulsed EPR distance measurements,[13] validating this extended conformation of the peptide. The general validity of this approach is also illustrated by a previous ssNMR study of a receptor-bound peptide,[34] whose extended conformation was later also observed in the X-ray structure of the receptor−peptide complex.[35] In conclusion, DNP ssNMR spectroscopy enabled the elucidation of an extended backbone conformation of 9-mer peptides bound to the translocation complex TAP.

Peptide Binding Site at the TAP1-TAP2 Interface. On the basis of the experimentally derived backbone conformation of a TAP-bound peptide, we docked the peptide substrate KRYQNSTVY into a structural model of the human TAP transporter. The structural model exploited the homology to the TAP-related heterodimeric ABC transport complex TmrAB.[36] Repeated docking produced a relatively tight bundle of peptides that bind to the TAP-TMDs in a slightly tilted orientation with respect to the normal of the membrane plane (Figures 6a and S4a). In the dominant binding mode, the N-terminal region interacts with a negatively charged pocket in TAP1, in particular with the TM3 residues $E290^{TAP1}$, $D297^{TAP1}$, and $E301^{TAP1}$ (Figure 6c and Table S5). By contrast, the C terminus of the peptide substrate is mainly in contact with residues of TAP2 (Figure 6b). Within the dominant cluster of docked peptides (Figure 6a), the C terminus interacts with a group of hydrophobic and basic residues, in particular $W413^{TAP1}$ in TM5, $R210^{TAP2}$ in TM2, and $K277^{TAP2}$ in TM3. It is important to note that a large cavity between the two half-transporters provides additional space for binding of peptides with bulky side chains (fluorophores, chemical proteases, or polylysine chains) or of long peptides with up to 40 amino acids,[13,37−39] which are expected to adopt a kinked conformation (Figure S4b).

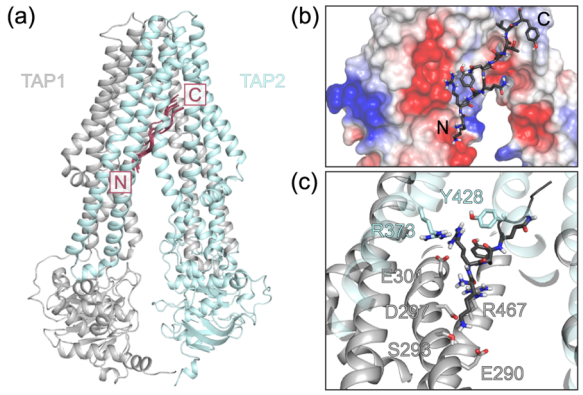

Figure 6. Mapping of the substrate binding site of the TAP complex. (a) Dominant cluster of docked peptides (10 poses, raspberry) bound to TAP (TAP1: gray, TAP2: cyan). (b) Electrostatic surface charge of TAP1. The N-terminal part of a representative docked peptide is interacting with a negatively charged pocket within the interior of the transmembrane domain of TAP1 (red: negative, blue: positive, white: neutral). (c) Interaction sites of the peptide−TAP complex. Residues within the TAP complex coordinating the N-terminal part of the peptide are shown as sticks (red: O, blue: N, white: H).

DISCUSSION

Here, we derived the backbone conformation of a peptide in complex with human TAP based on DNP-enhanced ssNMR data. These experiments represent the first NMR study of a human transport complex of low abundance, which can only be carried out thanks to the sensitivity enhancement provided by DNP as well as an optimized approach in sample preparation. The observed chemical shift changes pinpoint N and C termini as binding hotspots for TAP recognition. In complex with TAP, the peptide is in an overall extended conformation with an N-to-C terminus distance of ∼2.5 nm, which is in perfect agreement with pulsed EPR distance measurements on the TAP complex.[13] The binding affinity is significantly reduced for 8-mer peptides displaying identical amino acids at positions 1−3 and the C terminus (Figure 1a), underscoring a structural impact for the length selectivity by TAP. The affinity and specificity are mediated by multiple recognition sites in the N- and C-terminal regions. In particular, Lys1, Tyr3, and Tyr9 side chains are most substantially affected upon binding to TAP, revealing recognition principles of the translocation machinery. The N-terminal amino group shows a large downfield ^{15}N chemical shift change upon binding (Figure 4) and supports the formation of hydrogen bonds. This explains previous results that methylation of the α-amino group impairs peptide binding to TAP.[12] The α-amino group also shows another NMR peak in the bound state, which experiences only a minor ^{15}N chemical shift change (Figure 4). On the basis of our competition assay, we can exclude the dissociation of peptide from TAP. Therefore, peak splitting reveals a different binding mode of the peptide involving this site, which can be explained by either a variety of interaction sites or a transient, low-affinity bound state resembling the first binding step of the two-step binding process deciphered by peptide binding kinetic analysis.[40] We also observed some chemical shift/line width changes on Tyr3 and Tyr9 side chains, whose origin remains ambiguous and could be attributed plausibly to π-stacking interactions or hydrogen bridging of the hydroxyl group or even both. Interestingly, the guanidinium group of Arg2, which was supposed to be part of the interaction site, is merely influenced compared to other sites. The presented NMR data support the interaction of TAP with the N and C termini of the peptide substrate, which are decisive for the peptide sequence specificity driven by high-affinity binding.

The major destinations of the translocated antigen peptides are MHC I molecules in the ER lumen. Extensive X-ray crystallography studies have shown a rather fixed distance between the N and C termini of MHC I-bound peptides, defining the minimal length of MHC I ligands.[41] Interestingly, this distance resembles the N-to-C distance in the TAP-bound peptide as determined in this study (Figure 7a,b). Our findings point to a co-evolution between the TAP transporter and MHC I molecules. Functionally, TAP filters out short peptides, which cannot bind to MHC I anyway.

The mechanism of viral immune evasion by the viral inhibitor ICP47 was determined based on previous NMR studies[42,43] and a recent single-particle cryo-EM analysis.[44] The viral inhibitor shares a large interface with TAP, thus leading to a kinetically stable, high-affinity binding.[45] Peptide−TAP complex formation relies on a few anchor residues, resulting in a significantly faster off-rate compared to the viral TAP

DOI: 10.1021/jacs.6b07426
J. Am. Chem. Soc. 2016, 138, 13967−13974

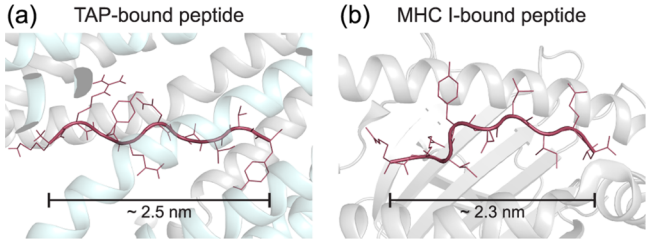

Figure 7. Co-evolution of proteins involved in antigen processing. Peptides bound to the TAP complex (a) display a similar N-to-C distance of 2.5 nm compared to MHC I-bound peptides, (b) with a distance of 2.3 nm (PDB: 2BSR, gray). TAP1: gray, TAP2: cyan.

inhibitor.[26] In contrast to ICP47, which requires a structural preorganization into an α-helical conformation,[42] peptides bind to TAP without any prefolded secondary structure motifs. Moreover, ICP47 mainly contacts transmembrane helices of TAP2,[44] whereas this study reveals the antigenic peptide primarily interacting with TAP1.

Molecular modeling and docking showed that the peptide substrate, locked with its N and C termini between TAP1 and TAP2, adopts a tilted pose with respect to the membrane plane (Figure 6a). Both half-transporters, TAP1 and TAP2, interact with the bound substrate and thus the heterodimer is required for high-affinity binding, consistent with former findings on homodimeric complexes lacking functionality.[46,47] A cluster of acidic residues within the transmembrane part of TAP1 casts a binding platform offering multiple interaction sites (Figure 6b,c). Indeed, the splitting of N-terminal amine NMR signals (Figure 4a) shows that the N-terminal peptide anchor populates distinct substates, consistent with local variations among the different binding poses obtained by docking. The depicted contact sites of TAP are also consistent with the findings of earlier studies on human TAP and its rat homologue (Table S5). Residues of TAP interacting with peptide substrates, as identified previously by cross-linking (Gly282, Ile284, Arg287, Val288,[37] Ser296, and Glu459[48] of human TAP1 and Cys213 of TAP2[49]), occupy the same locations as residues identified by our docking, e.g., $Glu290^{TAP1}$, $Asp297^{TAP1}$, $Arg467^{TAP1}$, and $Arg210^{TAP2}$ (Figure S4c). Providing additional support for the model, mutational analysis identified residues that affect substrate specificity and thus may take part in substrate binding, such as $Tyr408^{TAP1}$,[48] $Thr217^{TAP2}$/$Met218^{TAP2}$, $Ala374^{TAP2}$/$Arg380^{TAP2}$,[48,50−52] and $Asn262^{TAP2}$/$Pro265^{TAP2}$/$Leu266^{TAP2}$[52] (Figure S4d). Molecular docking thus provides structural details that help us rationalize earlier results on substrate specificity and binding.

CONCLUSIONS

In summary, we determined the backbone conformation of a peptide in complex with the human ABC transporter TAP by applying DNP-enhanced ssNMR. By elucidating the structure of the bound peptide and its interactions with TAP, we shed light on the strategies evolved in TAP for substrate recognition and optimized specificity. Our study also demonstrates that DNP-enhanced solid-state NMR allows challenging molecular questions to be addressed that would not be accessible by conventional NMR.

METHODS

Materials. Glyco-diosgenin (GDN) was purchased from Anatrace. Fmoc-protected amino acids and (1-cyano-2-ethoxy-2-oxoethylidenaminooxy) dimethylamino-morpholino-carbenium hexafluoro-phosphate (COMU) were obtained from Iris Biotech GmbH. Uniformly ^{15}N,^{13}C-labeled Fmoc amino acids and glycerol-d_8 were acquired from CortecNet and Euriso-Top. AMUPol was purchased from Aix-Marseille Université (Prof. Paul Tordo and Dr. Olivier Quari). All other chemicals were from Sigma-Aldrich, Carl Roth, and Merck.

Expression and Purification of TAP. Human TAP composed of coreTAP1 (Q03518, residues 224−808) carrying a TEV cleavage site followed by mCerulean and a His_{10}-tag at the C terminus and coreTAP2 (Q59H06, residues 124−687) fused to a TEV cleavage site, mVenus, and a StrepII-tag was expressed in *Pichia pastoris*.[53,54] Crude membrane preparation and TAP purification via IMAC were performed as described,[21] whereas 2 or 0.05% (w/v) glyco-diosgenin (GDN) was used for solubilization and further purification, respectively. Purified TAP was stored at −80 °C in GDN buffer (20 mM HEPES, 200 mM NaCl, 50 mM KCl, 15% (w/v) glycerol, 0.05% (w/v) GDN, pH 7.4).

Peptide Synthesis. Peptides were synthesized on a 2-chlorotrityl chloride polystyrene based resin applying a COMU-activated Fmoc solid-phase peptide synthesis strategy. The following side chain protecting groups were used: pentamethyl-2,3-dihydrobenzofuran-5-sulfonyl (Pbf) for arginine, *tert*-butyloxycarbonyl (Boc) for lysine, trityl (Trt) for glutamine and asparagine, and *tert*-butyl (*t*Bu) for tyrosine, serine, threonine, and glutamate. Deprotection was performed in 30% (v/v) piperidine. Finally, the peptide was cleaved from the resin with a mixture of 80% (v/v) trifluoroacetic acid, 5% (w/v) phenol, and 5% (v/v) each of 1,2-ethanedithiol, thioanisole, and water (Reagent K). Crude peptides were purified via RP-C_{18}-HPLC (PerfectSil 300 ODS C18, 5 μm, 250 × 10 mm, MZ-Analysentechnik GmbH) using a linear gradient of 5 to 30% (v/v) acetonitrile supplemented with 0.1% (v/v) trifluoroacetic acid. Pooled fractions were snap-frozen in liquid nitrogen and freeze-dried. Peptide purity and identity were verified by RP-C_{18}-HPLC and MALDI-TOF mass spectrometry.

Peptide Binding. The amount of bound peptide was determined by a filter-based binding assay. TAP (175 nM) was incubated with $RRYC^{F}KSTEL$ (labeled with fluorescein) for 20 min at 4 °C in GDN buffer. Background binding was measured in the presence of a 250-fold excess of a competitor peptide (RRYQKSTEL). Samples were transferred onto a filter plate (MultiScreen Filter Plate with Durapore Membrane, 0.65 μm, Merck Millipore) preincubated with 0.3% (w/v) polyethylenimine, washed twice with 250 μL of ice-cold GDN buffer, and incubated with 300 μL of elution buffer (phosphate buffered saline, 1% (w/v) SDS, pH 7.4) for 10 min. Samples were heated for 5 min at 95 °C to prevent interference of mVenus fluorescence. The amount of bound peptide was quantified by fluorescence at $\lambda_{ex/em}$ 485/520 nm. Equilibrium dissociation constants K_D were calculated by fitting the data with the Langmuir equation

$$B = \frac{B_{max} \cdot [C]}{K_D + [C]} \quad (1)$$

where B corresponds to the TAP-bound reporter peptide, B_{max} corresponds to the maximal amount of bound reporter, and C corresponds to the peptide concentration.

Binding affinities of optimized peptides were determined by competition experiments. Therefore, TAP (175 nM) was incubated with 1 μM $RRYC^{F}KSTEL$ and supplemented with increasing amounts of competitor peptide. Filter-based binding assays were performed as mentioned above. IC_{50} values were calculated from the corresponding dose−response curve according to the following equation

$$B = \frac{B_{max} - B_{bg}}{1 + 10^{[comp] - \log IC_{50}}} \quad (2)$$

whereas B_{bg} represents the background signal in a 250-fold excess of competitor (comp). The inhibition constant K_i was calculated with the Cheng−Prusoff equation and the corresponding K_D (50 nM) for the fluorescein-labeled reporter peptide.[21,55]

Dissociation Kinetics. Dissociation of the peptide−TAP complex was measured by fluorescence anisotropy on a Fluorolog-3

DOI: 10.1021/jacs.6b07426
J. Am. Chem. Soc. 2016, 138, 13967−13974

spectrometer (HORIBA Jobin Yvon GmbH). The anisotropy r is defined as

$$r = \frac{I_{\parallel} - G \cdot I_{\perp}}{I_{\parallel} + 2G \cdot I_{\perp}} \quad (3)$$

where $I_{\parallel}$ and $I_{\perp}$ are the parallel and perpendicular components of the fluorescence intensities, respectively. The G-factor for RRYC^{ATTO565}KSTEL (labeled with ATTO565) was determined prior to the anisotropy measurements with $\lambda_{ex/em}$ 563/592 nm.

To follow peptide dissociation, RRYC^{ATTO565}KSTEL (50 nM) was preincubated with TAP (1.35 μM) in GDN buffer at 4 °C until a stable anisotropy value was reached. Ligand dissociation was followed after the addition of a 1500-fold excess of unlabeled peptide. The decay in fluorescence anisotropy was fitted with a monoexponential function

$$r = r_{max}\, e^{-k_{diss}t} \quad (4)$$

NMR Sample Preparation. Active TAP (1.5 μM) was preincubated for 2 h at 4 °C with a 2-fold molar excess of isotope-labeled peptide in deuterated low-salt buffer (10 mM HEPES, 100 mM NaCl, 1% (w/v) $^{12}C_3$,$^{2}D_8$-glycerol, 10% (v/v) H_2O, 0.05% (w/v) GDN, pD 7.2). Free peptides were removed by gel filtration (PD10 column, GE Healthcare). Free peptide in low-salt buffer served as reference. Samples were supplemented with AMUPol (300 nmol), snap-frozen in 2-methylbutane precooled in liquid nitrogen, freeze-dried, and transferred into a 3.2 mm ZrO_2 MAS rotor via ultracentrifugation (120 000 × g, 30 min) at 4 °C. Each NMR sample contains 4.5 nmol of active TAP complex. The final AMUPol concentration was 10 mM.

DNP-Enhanced MAS ssNMR. All DNP-enhanced MAS ssNMR experiments were conducted on a Bruker Avance II spectrometer operated at 400.20 MHz (9.4 T) and equipped with a customized Bruker 3.2 mm HCN cryo-MAS probe head. High-power microwave (output power 24−29 W, 263.58 GHz) was generated in a CPI gyrotron and transmitted to the sample location via a corrugated waveguide. MAS was stabilized at 8000 ± 2 Hz at about 110 K in all measurements. Standard pulse sequences were used for recording DQ−SQ $^{13}C-^{13}C$ spectra using POST-C7[28] and TEDOR $^{15}N-^{13}C$ 2D experiments.[29,30] A DQ excitation time of 500 μs and a TEDOR mixing time of 1.0 ms were used. Referencing for ^{13}C chemical shifts was done indirectly to DSS using the low-field ^{13}C signal of adamantane at 40.49 ppm. ^{15}N chemical shifts were referenced indirectly to liquid ammonia. For all experiments, 100 kHz decoupling using SPINAL-64[56] was applied during acquisition. Further details regarding the spectral acquisition and processing are listed in Table S6.

Peptide Structural Calculation. Backbone torsion angle restraints were derived by TALOS-N using the backbone chemical shifts (N, CO, CA, and CB).[31] The amide ^{15}N chemical shifts of Asn5 to Val8 were not included due to their broad distributions. CYANA calculations were performed using the torsion angle restraints listed in Tables S3 and S4 without further constraints.[32] We performed 2000 calculations with a maximum of 20 000 steps for each calculation. The weight of torsion angle restrains was set to 0.05, a value allowing the calculation process to be well-guided by restraints. In total, 49 top solutions with zero or very small (<0.001) target functions were obtained. This set of solutions was chosen since their target functions were much lower than the other solutions (≥0.15), and this sharp gap presents a significant difference among the structure clusters. For presentation, we picked 10 representative conformations within these top solutions.

Homology Modeling and Docking. A set of sequence homologues of human TAP was obtained using the NCBI BLAST server against the nonredundant sequence database. These sequences were further filtered by selecting only unique sequences belonging to the branch of the phylogenetic tree that included either TAP1 or TAP2. This procedure resulted in 73 and 62 homologues of TAP1 and TAP2, respectively. Multiple sequence alignments of TAP1 and TAP2 homologues with TmrB and TmrA were then generated using PSI/TM-Coffee.[57] The initial multiple sequence alignments were accordingly refined by (i) considering the pairwise alignments between TAP1 and TAP2 with TmrB and TmrA, respectively, generated using AlignMe[58] and (ii) removing gaps in the secondary structure elements and the transmembrane regions guided by secondary structure prediction from PSIPRED[59] and transmembrane assignment from OCTOPUS.[60] Human TAP was modeled based on the X-ray crystal structure of TmrAB using Modeler 9v16[61] premised on the final sequence alignment. A single model was selected after generating 500 models with the best (i) MODELER score and (ii) PROCHECK[62] profile, which evaluates the stereochemistry. The selected homology model was prepared for the docking steps using Protein Preparation Wizard available in the Schrödinger package (v2016-1). The preparation steps were (i) addition of hydrogen atoms, (ii) adjustment of the ionization and tautomerization states of protein residues using PROPKA,[63] (iii) interactive optimization of the hydrogen-bonding network, and (iv) restrained minimization of the structure (within RMSD of 0.3 Å of initial model). Peptides were docked into the homology model of TAP using Glide v6.7.[64] A docking score developed for peptide docking (SP-Peptide) was used to rank different binding modes (poses).[65] During docking, all ϕ and ψ angles of the peptide backbone were constrained while side chains were flexible. Repeated docking attempts yielded 62 final docking poses, which were clustered using the Jarvis−Patrick method[66] implemented in the g_cluster command of GROMACS v4.6.5.[67] The dominant cluster depicted in Figure 6a contains 10 structures.

■ ASSOCIATED CONTENT

Supporting Information

The Supporting Information is available free of charge on the ACS Publications website at DOI: 10.1021/jacs.6b07426.

$^{13}C/^{15}N$ chemical shift assignment, torsion angle restraints from TALOS-N, residues within the substrate binding site revealed by peptide docking and previous studies, acquisition and processing parameters for ssNMR, purity and identity of isotope-labeled peptides, DQ−SQ $^{13}C-^{13}C$ and TEDOR $^{15}N-^{13}C$ ssNMR spectra, and additional docking results (PDF)

■ AUTHOR INFORMATION

Corresponding Authors

*glaubitz@em.uni-frankfurt.de (C.G.)

*tampe@em.uni-frankfurt.de (R.T.)

Author Contributions

‖E.L. and J.M. contributed equally to this work.

Notes

The authors declare no competing financial interest.

■ ACKNOWLEDGMENTS

We thank Dr. Sina Kazemi for initial help with CYANA calculations. We are grateful to Christine Le Gal for critically reading the manuscript. The German Reserach Foundation (SFB807, EXC115, and AB149/1) and the Max Planck Society (to A.R.M. and G.H.) supported this work.

■ REFERENCES

(1) ter Beek, J.; Guskov, A.; Slotboom, D. J. *J. Gen. Physiol.* **2014**, *143*, 419.

(2) Mayerhofer, P. U.; Tampé, R. *J. Mol. Biol.* **2015**, *427*, 1102.

(3) Blum, J. S.; Wearsch, P. A.; Cresswell, P. *Annu. Rev. Immunol.* **2013**, *31*, 443.

(4) Blees, A.; Reichel, K.; Trowitzsch, S.; Fisette, O.; Bock, C.; Abele, R.; Hummer, G.; Schäfer, L. V.; Tampé, R. *Sci. Rep.* **2015**, *5*, 17341.

(5) Koch, J.; Guntrum, R.; Heintke, S.; Kyritsis, C.; Tampé, R. *J. Biol. Chem.* **2004**, *279*, 10142.

(6) Koch, J.; Guntrum, R.; Tampé, R. *FEBS Lett.* **2006**, *580*, 4091.

DOI: 10.1021/jacs.6b07426
J. Am. Chem. Soc. 2016, 138, 13967−13974

(7) Nijenhuis, M.; Hämmerling, G. J. *J. Immunol.* **1996**, *157*, 5467.
(8) Ritz, U.; Drexler, I.; Sutter, D.; Abele, R.; Huber, C.; Seliger, B. *J. Immunol.* **2003**, *170*, 941.
(9) van Endert, P. M.; Tampé, R.; Meyer, T. H.; Tisch, R.; Bach, J. F.; McDevitt, H. O. *Immunity* **1994**, *1*, 491.
(10) Heemels, M. T.; Schumacher, T. N.; Wonigeit, K.; Ploegh, H. L. *Science* **1993**, *262*, 2059.
(11) Momburg, F.; Roelse, J.; Hämmerling, G. J.; Neefjes, J. J. *J. Exp. Med.* **1994**, *179*, 1613.
(12) Uebel, S.; Kraas, W.; Kienle, S.; Wiesmüller, K. H.; Jung, G.; Tampé, R. *Proc. Natl. Acad. Sci. U. S. A.* **1997**, *94*, 8976.
(13) Herget, M.; Baldauf, C.; Schölz, C.; Parcej, D.; Wiesmüller, K. H.; Tampé, R.; Abele, R.; Bordignon, E. *Proc. Natl. Acad. Sci. U. S. A.* **2011**, *108*, 1349.
(14) Maly, T.; Debelouchina, G. T.; Bajaj, V. S.; Hu, K.-N.; Joo, C.-G.; MakJurkauskas, M. L.; Sirigiri, J. R.; van der Wel, P. C. A.; Herzfeld, J.; Temkin, R. J.; Griffin, R. G. *J. Chem. Phys.* **2008**, *128*, 052211.
(15) Ni, Q. Z.; Daviso, E.; Can, T. V.; Markhasin, E.; Jawla, S. K.; Swager, T. M.; Temkin, R. J.; Herzfeld, J.; Griffin, R. G. *Acc. Chem. Res.* **2013**, *46*, 1933.
(16) Kaplan, M.; Cukkemane, A.; van Zundert, G. C.; Narasimhan, S.; Daniels, M.; Mance, D.; Waksman, G.; Bonvin, A. M.; Fronzes, R.; Folkers, G. E.; Baldus, M. *Nat. Methods* **2015**, *12*, 649.
(17) Frederick, K. K.; Michaelis, V. K.; Corzilius, B.; Ong, T. C.; Jacavone, A. C.; Griffin, R. G.; Lindquist, S. *Cell* **2015**, *163*, 620.
(18) Maciejko, J.; Mehler, M.; Kaur, J.; Lieblein, T.; Morgner, N.; Ouari, O.; Tordo, P.; Becker-Baldus, J.; Glaubitz, C. *J. Am. Chem. Soc.* **2015**, *137*, 9032.
(19) Becker-Baldus, J.; Bamann, C.; Saxena, K.; Gustmann, H.; Brown, L. J.; Brown, R. C.; Reiter, C.; Bamberg, E.; Wachtveitl, J.; Schwalbe, H.; Glaubitz, C. *Proc. Natl. Acad. Sci. U. S. A.* **2015**, *112*, 9896.
(20) Bowness, P. *Annu. Rev. Immunol.* **2015**, *33*, 29.
(21) Eggensperger, S.; Fisette, O.; Parcej, D.; Schäfer, L. V.; Tampé, R. *J. Biol. Chem.* **2014**, *289*, 33098.
(22) Bajaj, V. S.; van der Wel, P. C. A.; Griffin, R. G. *J. Am. Chem. Soc.* **2009**, *131*, 118.
(23) Gardiennet, C.; Schutz, A. K.; Hunkeler, A.; Kunert, B.; Terradot, L.; Bockmann, A.; Meier, B. H. *Angew. Chem., Int. Ed.* **2012**, *51*, 7855.
(24) Bertini, I.; Luchinat, C.; Parigi, G.; Ravera, E. *Acc. Chem. Res.* **2013**, *46*, 2059.
(25) Takahashi, H.; Hediger, S.; De Paepe, G. *Chem. Commun.* **2013**, *49*, 9479.
(26) Neumann, L.; Abele, R.; Tampé, R. *J. Mol. Biol.* **2002**, *324*, 965.
(27) Sauvée, C.; Rosay, M.; Casano, G.; Aussenac, F.; Weber, R. T.; Ouari, O.; Tordo, P. *Angew. Chem., Int. Ed.* **2013**, *52*, 10858.
(28) Hohwy, M.; Jakobsen, H. J.; Eden, M.; Levitt, M. H.; Nielsen, N. C. *J. Chem. Phys.* **1998**, *108*, 2686.
(29) Hing, A. W.; Vega, S.; Schaefer, J. *J. Magn. Reson.* **1992**, *96*, 205.
(30) Jaroniec, C. P.; Filip, C.; Griffin, R. G. *J. Am. Chem. Soc.* **2002**, *124*, 10728.
(31) Shen, Y.; Bax, A. *J. Biomol. NMR* **2013**, *56*, 227.
(32) Güntert, P.; Mumenthaler, C.; Wuthrich, K. *J. Mol. Biol.* **1997**, *273*, 283.
(33) Hafsa, N. E.; Wishart, D. S. *J. Biomol. NMR* **2014**, *60*, 131.
(34) Luca, S.; White, J. F.; Sohal, A. K.; Filippov, D. V.; van Boom, J. H.; Grisshammer, R.; Baldus, M. *Proc. Natl. Acad. Sci. U. S. A.* **2003**, *100*, 10706.
(35) White, J. F.; Noinaj, N.; Shibata, Y.; Love, J.; Kloss, B.; Xu, F.; Gvozdenovic-Jeremic, J.; Shah, P.; Shiloach, J.; Tate, C. G.; Grisshammer, R. *Nature* **2012**, *490*, 508.
(36) Nöll, A.; Thomas, C.; Herbring, V.; Zollmann, T.; Barth, K.; Mehdipour, A. R.; Tomasiak, T. M.; Brüchert, S.; Joseph, B.; Abele, R.; Olieric, V.; Wang, M.; Diederichs, K.; Hummer, G.; Stroud, R. M.; Pos, K. M.; Tampé, R. **2016**, submitted.
(37) Herget, M.; Oancea, G.; Schrodt, S.; Karas, M.; Tampé, R.; Abele, R. *J. Biol. Chem.* **2006**, *282*, 3871.
(38) Gorbulev, S.; Abele, R.; Tampé, R. *Proc. Natl. Acad. Sci. U. S. A.* **2001**, *98*, 3732.
(39) Koopmann, J. O.; Post, M.; Neefjes, J. J.; Hämmerling, G. J.; Momburg, F. *Eur. J. Immunol.* **1996**, *26*, 1720.
(40) Neumann, L.; Tampé, R. *J. Mol. Biol.* **1999**, *294*, 1203.
(41) Madden, D. R. *Annu. Rev. Immunol.* **1995**, *13*, 587.
(42) Aisenbrey, C.; Sizun, C.; Koch, J.; Herget, M.; Abele, R.; Bechinger, B.; Tampé, R. *J. Biol. Chem.* **2006**, *281*, 30365.
(43) Pfänder, R.; Neumann, L.; Zweckstetter, M.; Seger, C.; Holak, T. A.; Tampé, R. *Biochemistry* **1999**, *38*, 13692.
(44) Oldham, M. L.; Hite, R. K.; Steffen, A. M.; Damko, E.; Li, Z.; Walz, T.; Chen, J. *Nature* **2016**, *529*, 537.
(45) Ahn, K.; Meyer, T. H.; Uebel, S.; Sempé, P.; Djaballah, H.; Yang, Y.; Peterson, P. A.; Früh, K.; Tampé, R. *EMBO J.* **1996**, *15*, 3247.
(46) Meyer, T. H.; van Endert, P. M.; Uebel, S.; Ehring, B.; Tampé, R. *FEBS Lett.* **1994**, *351*, 443.
(47) Urlinger, S.; Kuchler, K.; Meyer, T. H.; Uebel, S.; Tampé, R. *Eur. J. Biochem.* **1997**, *245*, 266.
(48) Geng, J.; Pogozheva, I. D.; Mosberg, H. I.; Raghavan, M. *J. Immunol.* **2015**, *195*, 3436.
(49) Baldauf, C.; Schrodt, S.; Herget, M.; Koch, J.; Tampé, R. *Proc. Natl. Acad. Sci. U. S. A.* **2010**, *107*, 9135.
(50) Armandola, E. A.; Momburg, F.; Nijenhuis, M.; Bulbuc, N.; Früh, K.; Hämmerling, G. J. *Eur. J. Immunol.* **1996**, *26*, 1748.
(51) Momburg, F.; Armandola, E. A.; Post, M.; Hämmerling, G. J. *J. Immunol.* **1996**, *156*, 1756.
(52) Deverson, E. V.; Leong, L.; Seelig, A.; Coadwell, W. J.; Tredgett, E. M.; Butcher, G. W.; Howard, J. C. *J. Immunol.* **1998**, *160*, 2767.
(53) Schölz, C.; Parcej, D.; Ejsing, C. S.; Robenek, H.; Urbatsch, I. L.; Tampé, R. *J. Biol. Chem.* **2011**, *286*, 13346.
(54) Parcej, D.; Guntrum, R.; Schmidt, S.; Hinz, A.; Tampé, R. *PLoS One* **2013**, *8*, e67112.
(55) Cheng, Y.-C.; Prusoff, W. H. *Biochem. Pharmacol.* **1973**, *22*, 3099.
(56) Fung, B. M.; Khitrin, A. K.; Ermolaev, K. *J. Magn. Reson.* **2000**, *142*, 97.
(57) Chang, J. M.; Di Tommaso, P.; Taly, J. F.; Notredame, C. *BMC Bioinf.* **2012**, *13* (Suppl 4), S1.
(58) Stamm, M.; Staritzbichler, R.; Khafizov, K.; Forrest, L. R. *Nucleic Acids Res.* **2014**, *42*, W246.
(59) McGuffin, L. J.; Bryson, K.; Jones, D. T. *Bioinformatics* **2000**, *16*, 404.
(60) Viklund, H.; Elofsson, A. *Bioinformatics* **2008**, *24*, 1662.
(61) Šali, A.; Blundell, T. L. *J. Mol. Biol.* **1993**, *234*, 779.
(62) Laskowski, R. A.; Rullmann, J. A.; MacArthur, M. W.; Kaptein, R.; Thornton, J. M. *J. Biomol. NMR* **1996**, *8*, 477.
(63) Olsson, M. H.; Sondergaard, C. R.; Rostkowski, M.; Jensen, J. H. *J. Chem. Theory Comput.* **2011**, *7*, 525.
(64) Friesner, R. A.; Banks, J. L.; Murphy, R. B.; Halgren, T. A.; Klicic, J. J.; Mainz, D. T.; Repasky, M. P.; Knoll, E. H.; Shelley, M.; Perry, J. K.; Shaw, D. E.; Francis, P.; Shenkin, P. S. *J. Med. Chem.* **2004**, *47*, 1739.
(65) Tubert-Brohman, I.; Sherman, W.; Repasky, M.; Beuming, T. *J. Chem. Inf. Model.* **2013**, *53*, 1689.
(66) Jarvis, R. A.; Patrick, E. A. *IEEE Trans. Comput.* **1973**, *C-22*, 1025.
(67) Pronk, S.; Pall, S.; Schulz, R.; Larsson, P.; Bjelkmar, P.; Apostolov, R.; Shirts, M. R.; Smith, J. C.; Kasson, P. M.; van der Spoel, D.; Hess, B.; Lindahl, E. *Bioinformatics* **2013**, *29*, 845.

DOI: 10.1021/jacs.6b07426
J. Am. Chem. Soc. 2016, 138, 13967−13974